

Ferromagnetic phase of spinel compound MgV_2O_4 and its spintronics properties

Javad G. Azadani,¹ Wei Jiang,^{1,*} Jian-Ping Wang,¹ and Tony Low^{1,†}

¹*Department of Electrical and Computer Engineering,
University of Minnesota, Minneapolis, Minnesota 55455, USA*

Spinel compound, MgV_2O_4 , known as a highly frustrated magnet has been extensively studied both experimentally and theoretically for its exotic quantum magnetic states. However, due to its intrinsic insulating nature in its antiferromagnetic (AFM) ground state, its realistic applications in spintronics are quite limited. Here, based on first-principles calculations, we examine the ferromagnetic (FM) phase of MgV_2O_4 , which was found to host three-dimensional flat band (FB) right near the Fermi level, consequently yielding a large anomalous Hall effect (AHE, $\sigma \approx 670 \Omega^{-1} \cdot \text{cm}^{-1}$). Our calculations suggest that the half-metallicity feature of MgV_2O_4 is preserved even after interfacing with MgO due to the excellent lattice matching, which could be a promising spin filtering material for spintronics applications. Lastly, we explore experimental feasibility of stabilizing this FM phase through strain and doping engineering. Our study suggests that experimentally accessible amount of hole doping might induce a AFM-FM phase transition.

INTRODUCTION

Spinel compounds, with a large family of interesting magnetic materials, have been extensively studied for decades for their rich magnetic¹⁻⁴, electronic^{5,6}, optical⁷, and topological properties^{8,9}. In general, spinel compounds with chemical formula $A_{1-\alpha}B_\alpha(A_\alpha B_{2-\alpha})X_4$ are classified into the normal ($\alpha = 0$), inverse ($\alpha = 1$), and complex ($0 < \alpha < 1$), depending on the different cations (A and B) distributions in octahedral and tetrahedral locations. The most widely investigated spinels are normal spinels with chemical formula AB_2X_4 , where the A and B metal cations are located at the tetrahedral and octahedral sites, respectively. The conventional unit cell is presented in Fig. 1(a), where X ions form the face-centered cubic lattice and cations A and B form diamond and three-dimensional (3D) kagome sublattices, respectively.

For the system to be charge neutral, anion X always accept two electrons while cations A normally donates two or four electrons and cations B donates two or three electrons, leading to the two possible $A^{4+}B_2^{2+}X_4^{2-}$ or $A^{2+}B_2^{3+}X_4^{2-}$ states. Therefore, with combinations of different cations A and B, we are able to selectively populate different sublattices. For example, within vanadium spinels, $V^{4+}\text{Mg}_2^{2+}\text{O}_4$ shows interesting magnetic Weyl semimetal state due to the diamond lattice constructed by V^{4+} ions⁹; while $\text{Mg}^{2+}\text{V}_2^{3+}\text{O}_4$ is a well known highly frustrated magnet that hosts intriguing quantum magnetic states due to the corner-sharing 3D kagome lattice¹⁰. Both of these spinels, in principle, could be experimentally synthesized by properly controlling the oxygen pressure and stoichiometric ratio between the elements¹¹⁻¹⁴. Nevertheless, the commonly observed phase experimentally is $\text{Mg}^{2+}\text{V}_2^{3+}\text{O}_4$, which is intrinsically an anti-ferromagnetic (AFM) insulator¹⁰. Studies on other spinel compounds, such as ZnCr_2O_4 and CaCr_2O_4 , suggest hole doping can stabilize the ferromagnetic (FM) phase¹⁵⁻¹⁸. However, the electronic properties of the MgV_2O_4 in its FM phase is not well understood. Here we reveal that the FM phase can accom-

modates interesting topological and spintronics properties. This includes large anomalous Hall conductivity, half metallicity, and AFM-FM and metal-insulator transitions. We also explore possible strain and doping approaches where this FM phase might be stabilize, which can motivate its experimental search.

In this work, we revisit the electronic and magnetic properties of MgV_2O_4 with first-principles calculations based on density functional theory (DFT). A significant point of departure of our work to prior literature is the emphasis on its 3D kagome lattice, and its characteristic flat band (FB). FBs are well studied in the literatures for their interesting physics such as superconductivity^{19,20}, ferromagnetism²¹⁻²⁴ and topological states²⁵⁻²⁹. The FM MgV_2O_4 shows interesting FB feature and ideal half-metallicity with a large spin gap, which is further analysed based on tight-binding simulation of the 3D kagome lattice model. We found that intrinsic AFM MgV_2O_4 could transition into a FM state via experimentally accessible hole doping, such as ionic gel gating. Interestingly, the AFM to FM transition is accompanied with an insulator to metal transition and a giant variation of anomalous Hall effect. Lastly, we demonstrated how lattice and chemically matched interface between MgV_2O_4 and MgO could help to preserve its half-metallicity. These new predictions could potentially usher in future novel and practical spintronics applications.

FIRST-PRINCIPLES CALCULATION RESULTS

We start by studying the electronic properties of MgV_2O_4 in the FM state rather than commonly studied AFM phase (Supplemental Material³⁰). To treat the strongly localized d electrons of V ions, an on-site Hubbard U term is added. Using the documented value ($U=3.0\text{eV}$)^{31,32}, spin-polarized band structure for FM MgV_2O_4 is presented in Fig. 1(c), which interestingly shows an ideal half-metallic feature with a large band gap of 4.15 eV for the spin-down channel. The half-metallicity will remain for different U values, which only changes the

separation between two spin channels³⁰. For example, in Fig. 1(c), the minority spin (red) bands are separated from the majority spin (blue) Fermi surface by about 1 eV. Moreover, MgV_2O_4 possesses four nearly FBs right above the Fermi energy, with their bandwidths varying from 29 meV (very flat) to 205 meV. Detailed analysis show that there are two three-fold degenerated points formed by two FBs and one dispersive band at the center of Brillouin zone (BZ), (Γ) at energies 16 meV and 196 meV above the Fermi level, respectively.

To reveal the nature of these FBs, we calculated orbital and orbital-projected density of states (PDOS), as shown in Fig. 1(d). Around the Fermi level, there is a sharp peak that corresponds to the FBs. These FBs are mainly contributed by spin up electrons of the vanadium atoms, which form the 3D kagome lattice. This agrees with the magnetic moment distribution, which are mainly localized on V atoms. Detailed analysis of PDOS shows that all the twelve bands near the Fermi level ($E_F - 1.88$ to $E_F + 0.22$ eV) are contributed by the t_{2g} orbitals. This can be understood from the crystal field splitting of the V atoms in the octahedron formed by neighboring O ions, which splits the five degenerate d orbitals into two e_g and three t_{2g} orbitals with relatively lower energy. Due to the slight distortion of the octahedron, three degenerate t_{2g} orbitals are further splitted into one lower energy d_{xy} and two nearly degenerate d_{xz} and d_{yz} orbitals, which is further validated by the different O-V bond angle in the octahedron³⁰. After donating two s and one d electrons, V^{3+} ions have two d electrons left. Therefore, with the remaining two valence electrons of V^{3+} , the d_{xy} orbitals with the lowest energy will be fully filled while the other two degenerate d_{xz} and d_{yz} orbitals will be half-filled.

In forming the band structure, each d orbitals will, in principle, form one set of 3D kagome lattice, and the band filling will be determined by the number of valence electrons of V. These indeed agree perfectly with the band structure from DFT, where the bottom set of 3D kagome bands are fully occupied and the upper eight bands are half filled, which correspond to the two sets of 3D kagome bands. We note that the large difference of the band width between those 3D kagome bands is due to the distortion induced changes of the hopping t for different d orbitals. We also performed maximally localized Wannier functions (MLWFs) calculations using the WANNIER90 package³³. As shown in Fig. 1(c), the MLWF fitted band structure agrees perfectly with the DFT band structure. The plotted MLWFs further validate the orbital characteristics of vanadium atoms [see Fig. 1(b)].

With the increasing interest in spintronics, materials with ideal half-metallicity and large spin/anomalous Hall effect are extensively studied. However, materials with both of those features are still quite rare. The ideal half-metallicity of the FM MgV_2O_4 has already been demonstrated from the electronic band structure, which shows a spin gap as large as 4.15 eV. Further, we study the

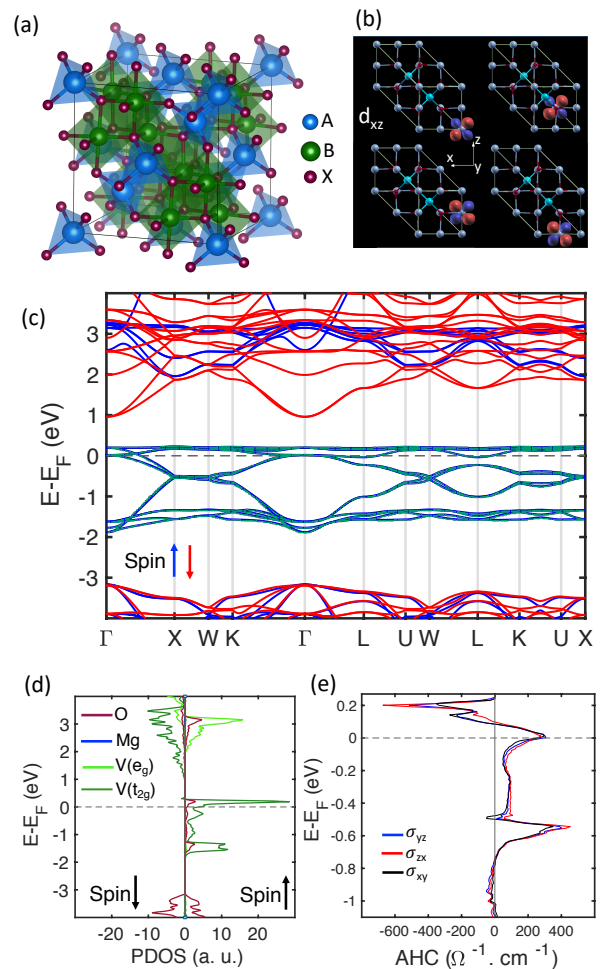


Figure 1. First-principles calculations. (a) Conventional crystal structure of spinel compound with formula AB_2X_4 , where metals A and B occupy the centers of tetrahedrons (blue) and octahedrons (green), respectively. (b) Maximally localized Wannier functions showing d_{xz} orbitals of four vanadium atoms in the lattice. (c) Band structure of MgV_2O_4 in its FM state, where blue and red colors corresponds to the spin-up and spin-down channels, respectively. MLWF fitted bands is overlaid with green dotted lines. (d) Projected density of states (PDOS) of MgV_2O_4 , showing the strong contribution of t_{2g} orbitals of vanadium atoms around the Fermi level. The zero of the energy is set to the Fermi energy. (e) Anomalous Hall conductivity (AHC) plotted, showing large peaks of $670 \Omega^{-1} \cdot \text{cm}^{-1}$ and $450 \Omega^{-1} \cdot \text{cm}^{-1}$ at 0.20 eV above and 0.54 eV below the Fermi energy, respectively. The magnetization direction is along (111).

anomalous Hall effect by calculating the anomalous Hall conductivity (AHC). First, we recalculate the band structure of MgV_2O_4 by turning on the spin-orbit coupling (SOC) and then fit the results using MLWFs, based on which a tight-binding Hamiltonian is obtained³⁰. The AHC can be acquired by integrating the Berry curvature of the occupied bands. We plotted the energy-dependent

AHC of MgV_2O_4 , as shown in Fig. 1(e). It can be clearly seen a large AHC peak of $670 \Omega^{-1} \cdot \text{cm}^{-1}$ at 0.20 eV above the Fermi energy is observed, which can be traced to the 3D FBs. There is also a large AHC of $450 \Omega^{-1} \cdot \text{cm}^{-1}$ at energy 0.54 eV below the Fermi energy. Note that the three components of AHC have relatively similar values, which is related to the direction of magnetization, that is along (111) direction. The large AHC can arise from the large Berry curvatures and electronic topology of the 3D kagome lattice, which only present in the FM state of MgV_2O_4 . Detailed analysis about the AHC is beyond the scope of this work, which will be discussed in a separate study³⁴.

TIGHT-BINDING ANALYSIS

Since the bands of interest are mainly contributed by vanadium d electrons, we can better understand the formation of the FB by analyzing the tight-binding model on a 3D kagome lattice. The primitive unit cell of the 3D kagome lattice contains four atomic states, with one corner-site and three edge-center-site states as presented by green atoms (B) in Fig. 2(a). Here, \vec{a} , \vec{b} , and \vec{c} are the three primitive vectors pointing between nearest-neighbor (NN) lattice points that form a tetrahedron. It can be seen that the cross section along each of the four faces of the tetrahedron produces one 2D kagome lattice, as shown in Fig. 2(b), and for this we dubbed the system 3D kagome lattice. The first BZ of this lattice with high-symmetry lines is shown in Fig. 2(c). For simplicity, we consider one state per lattice site and only take NN interactions into account in our model. The spinless Hamiltonian is written as

$$H = \sum \epsilon_i c_i^\dagger c_i + \sum_{\langle ij \rangle} t c_i^\dagger c_j + H.c., \quad (1)$$

where ϵ_i is the on-site energy that is set as zero, and $\langle ij \rangle$ denotes summation over NN sites. c_i^\dagger (c_j) creates (annihilates) an electron on the site \vec{r}_i (\vec{r}_j), and NN hopping t are set as the same value for all the NNs considering the structural symmetry.

By diagonalizing the Hamiltonian, we obtain the analytical energy bands as $E_{1,2} = -2t(1 \pm \sqrt{1 + A})$ and $E_{3,4} = 2t$. A is given by $A = \cos(2k_x) \cos(2k_y) + \cos(2k_x) \cos(2k_z) + \cos(2k_y) \cos(2k_z)$, where $\vec{k} = (k_x, k_y, k_z)$ is the reciprocal lattice vector. The band structure along high-symmetry k-paths is shown in Fig. 2(d), which shows clearly the completely dispersionless FBs with double degeneracy located on top of two dispersive bands. The FBs touch the dispersive band at the Γ point, forming a triple degenerate point, and the two dispersive bands construct the nodal lines along diagonal directions of the square face of BZ (i.e. X-W line). These agree with the calculated band structure of MgV_2O_4 . When considering two d orbitals with slightly

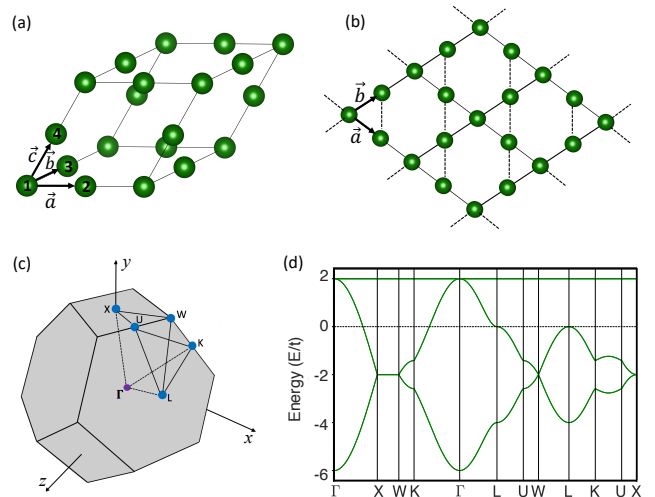


Figure 2. Tight-binding analysis on 3D Kagome lattice. (a) Primitive unit cell of the pyrochlore lattice, where only atoms which form a 3D Kagome lattice are shown. (b) Cross section along each of the four faces of the tetrahedron produces one 2D kagome lattice, which one of them (a - b plane) is shown here. (c) The first Brillouin zone of the 3D kagome lattice with high-symmetry points and lines indicated. (d) Tight-binding band structure of 3D Kagome lattice, containing two-fold degenerate flat bands at $E = 2t$, where t is hopping amplitude for NN interactions.

different on-site energy, we are able to reproduce the DFT band structure³⁰.

METAL TO INSULATOR TRANSITION

However, MgV_2O_4 is known to have a frustrated AFM ground state, which possesses an insulating state with different electronic properties than the FM case^{32,35,36}. In contrast to the FM state, 3D FBs are absent in the AFM ground state of MgV_2O_4 . We seek to engineer the magnetic ground state of MgV_2O_4 based on DFT calculations. It is worth mentioning that SOC and on-site Coulomb interaction are known to be important for the properties of MgV_2O_4 ³² and thus all are included in our calculations (see calculation details in Ref.³⁰). First, the total energy of the intrinsic MgV_2O_4 in the FM and AFM states are calculated, which shows that AFM energy, E_{AFM} is about 0.93 eV lower than FM state, E_{FM} , in agreement with previous studies^{10,14}. There are several approaches to tuning the magnetic state, e.g., chemical doping, structural engineering, or external magnetic field^{37,38}. The magnetic field required to change the magnetic state depends on the exchange coupling strength, which is usually hard to manipulate and impractical for devices. Therefore, we focus on the chemical doping and lattice engineering methods.

The strain engineering is accomplished through changing the lattice constant of MgV_2O_4 . We calculated

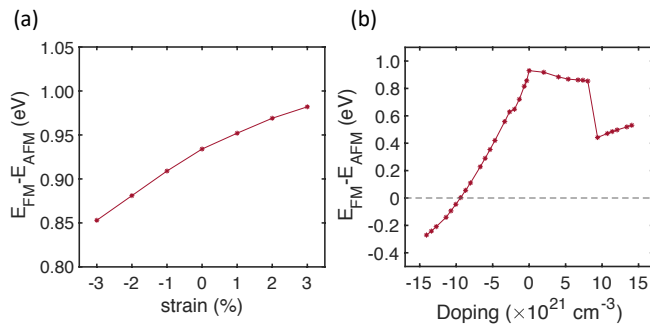


Figure 3. Engineering the magnetic ground state of MgV_2O_4 . (a) Energy difference between FM and AFM states versus different values of anisotropic strain along y -direction. MgV_2O_4 remains to be AFM for all values of strains. (b) Energy difference between non-collinear calculations of FM and AFM states versus doping concentration, where positive and negative values corresponds to electron and hole doped MgV_2O_4 , respectively. Hole doping of $10 \times 10^{21} \text{ cm}^{-3}$ switches the magnetization of MgV_2O_4 to the FM.

the E_{FM} and E_{AFM} after applying both isotropic and anisotropic strains. However, within the experimental accessible range, the ground state of MgV_2O_4 remains to be AFM, as shown in Fig. 3(a). To study the doping effect, we doped the system by changing the total number of electrons of the system while maintaining the charge neutrality with a compensating homogeneous background charge. E_{FM} and E_{AFM} for both hole and electron doping scenarios are calculated. As shown in Fig. 3(b), the system remains to be AFM for electron doping while changes to FM with the hole doping of $1 \times 10^{22} \text{ cm}^{-3}$. We note that this doping concentration is experimentally feasible, which can be achieved through either element substitution or ionic gel gating methods^{39,40}. It is also important to mention that apart from a rigid shift of its Fermi level, characteristic band features are preserved after doping, i.e., the 3D kagome bands³⁰. Therefore, hole doping leads to an insulator-to-half metal transition for MgV_2O_4 , which is consistent with previous experimental observations with Li doping of $\text{Li}_x\text{Mg}_{1-x}\text{V}_2\text{O}_4$ ¹⁸.

Considering the large variety of the spinel compounds, it should also be possible to find another compounds with FM ground state that host 3D FBs. Such hole doping induced AFM to FM transition has also been reported in chromium (III) spinels^{16,17}, which could possibly arise due to the breakdown of magnetic frustration, leading to the transition from long-range AFM coupling to short-range FM ordering. Considering the insulating feature of the AFM state without FBs, it is reasonable to expect a negligible AHC in the intrinsic MgV_2O_4 without hole doping. Therefore, through the hole doping, we actually accomplish a metal to insulator transition with a dramatic change of the AHE simultaneously. We note that due to the limitation of standard DFT in dealing with strong-correlated electrons, exact doping concentration to induce such phase transition from AFM to FM might

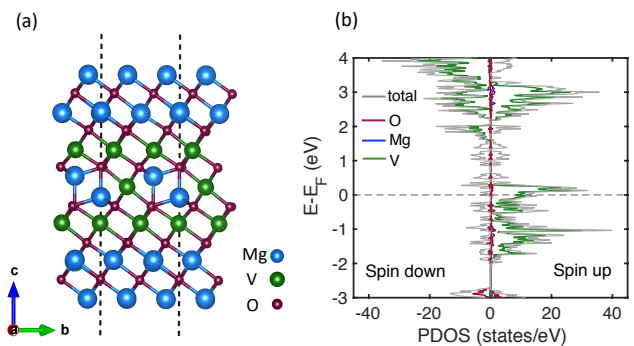


Figure 4. (a) $\text{MgO}/\text{MgV}_2\text{O}_4/\text{MgO}$ supercell. (b) Projected DOS of spacer layer MgV_2O_4 and total DOS of MgV_2O_4 and MgO heterostructure, showing robust and complete spin polarization of MgV_2O_4 after integrating with MgO .

varies, but the qualitatively phase transition should be valid as already demonstrated by related experiments³⁶. Nevertheless, within the standard DFT formalism where electrons correlations are treated in a Hartree-Fock mean field manner, we conclude hole doping to be the most effective and feasible approach to experimentally access the intriguing FM state of MgV_2O_4 .

HALF-METALLICITY INTERFACE

Finally, it should be noted that MgV_2O_4 has a very small lattice mismatch of $\sim 0.7\%$ with MgO , and a similar structure, yielding a smooth interface with MgO . Therefore, it could be used as a spacer layer in magnetic tunnel junction (MTJ) devices, as shown in Fig. 4(a), or as a spin filtering layer⁹. To demonstrate this possibility, we directly simulate the $\text{MgO}/\text{MgV}_2\text{O}_4/\text{MgO}$ heterostructure along (111) direction with three V layers. Interestingly, MgV_2O_4 remains a half-metal even after integrating with MgO . Figure 4(b) presents total DOS of the heterostructure and PDOS of MgV_2O_4 layer in the supercell, which shows an almost complete spin polarization for the sandwiched MgV_2O_4 layer.

SUMMARY

In this paper, by using first-principles calculations, we studied the experimentally synthesized MgV_2O_4 spinel compound and observed interesting 3D FBs in its FM phase. Vanadium atoms reside at the center of octahedrons forms a geometric frustrated 3D kagome lattice, which give rise to the 3D FBs right above the Fermi energy. PDOS calculations revealed that vanadium t_{2g} orbitals contribute to the FBs, which was further confirmed by MLWFs calculations. Through hole doping, MgV_2O_4 with the insulating AFM ground state can be tuned into FM state, which is an ideal half-metal. Inter-

estingly, the FBs contribute to a giant anomalous Hall effect right above the Fermi level. We believe these findings can greatly enrich the materials that have 3D FB, which could facilitate future experimental validation. Also, the FM-AFM (half-metal-insulator) transition with tunable AHE will also broaden the application of spinel compounds in spintronics.

ACKNOWLEDGEMENTS

This work is supported by SMART, one of seven centers of nCORE, a Semiconductor Research Corporation

program, sponsored by National Institute of Standards and Technology (NIST). We acknowledge computational support from the Minnesota Supercomputing Institute (MSI).

* jiangw@umn.edu

† tlow@umn.edu

- ¹ Raul Valenzuela. Novel applications of ferrites. *Physics Research International*, 2012, 2012.
- ² José F Marco, J Ramón Gancedo, Mercedes Gracia, Juan Luis Gautier, Edmundo I Ríos, Helen M Palmer, Colin Greaves, and Frank J Berry. Cation distribution and magnetic structure of the ferrimagnetic spinel NiCo_2O_4 . *Journal of Materials Chemistry*, 11(12):3087–3093, 2001.
- ³ Sukon Phanichphant et al. Cellulose-precursor synthesis of nanocrystalline $\text{Co}_{0.5}\text{Cu}_{0.5}\text{Fe}_2\text{O}_4$ spinel ferrites. *Materials Research Bulletin*, 47(2):473–477, 2012.
- ⁴ Qing Zhao, Zhenhua Yan, Chengcheng Chen, and Jun Chen. Spinel: controlled preparation, oxygen reduction/evolution reaction application, and beyond. *Chemical reviews*, 117(15):10121–10211, 2017.
- ⁵ Yonghyun Cho, Sanghan Lee, Yongseok Lee, Taeun Hong, and Jaephil Cho. Spinel-layered core-shell cathode materials for Li-ion batteries. *Advanced Energy Materials*, 1(5):821–828, 2011.
- ⁶ A Nirmallesh Naveen, P Manimaran, and S Selladurai. Cobalt oxide (Co_3O_4)/graphene nanosheets (gns) composite prepared by novel route for supercapacitor application. *Journal of Materials Science: Materials in Electronics*, 26(11):8988–9000, 2015.
- ⁷ Noriyuki Sonoyama, Ken Kawamura, Atsuo Yamada, and Ryoji Kanno. Electrochemical luminescence of rare earth metal ion doped MgIn_2O_4 electrodes. *Journal of The Electrochemical Society*, 153(3):H45–H50, 2006.
- ⁸ Gang Xu, Hongming Weng, Zhijun Wang, Xi Dai, and Zhong Fang. Chern semimetal and the quantized anomalous hall effect in HgCr_2Se_4 . *Phys. Rev. Lett.*, 107:186806, Oct 2011.
- ⁹ Wei Jiang, Huaqing Huang, Feng Liu, Jian-Ping Wang, and Tony Low. Magnetic weyl semimetals with diamond structure realized in spinel compounds. *Physical Review B*, 101(12):121113, 2020.
- ¹⁰ Elisa M Wheeler, Bella Lake, ATM Nazmul Islam, Manfred Reehuis, Paul Steffens, Tatiana Guidi, and Adrian H Hill. Spin and orbital order in the vanadium spinel MgV_2O_4 . *Physical Review B*, 82(14):140406, 2010.
- ¹¹ Hirotoshi Oshima. Phase relations in the system $\text{MgO-V}_2\text{O}_3\text{-VO}_2$ at 1200 °C. *Journal of the American Ceramic Society*, 63(9-10):504–508, 1980.
- ¹² John R. Hellmann and Vladimir S. Stubican. Phase relations and ordering in the systems $\text{MgO-Y}_2\text{O}_3\text{-ZrO}_2$ and CaO-MgO-ZrO_2 . *JACS*, 66(4):265–267, 1983.
- ¹³ ATM Nazmul Islam, Elisa M Wheeler, Manfred Reehuis, Konrad Siemensmeyer, Michael Tovar, Bastian Klemke, Klaus Kiefer, Adrian H Hill, and Bella Lake. Growth and magnetic properties of stoichiometric and site-disordered single crystalline MgV_2O_4 . *Physical Review B*, 85(2):024203, 2012.
- ¹⁴ S Niitaka, H Ohsumi, K Sugimoto, S Lee, Y Oshima, K Kato, D Hashizume, T Arima, M Takata, and H Takagi. A-type antiferro-orbital ordering with I 41/a symmetry and geometrical frustration in the spinel vanadate MgV_2O_4 . *Physical review letters*, 111(26):267201, 2013.
- ¹⁵ Z Zhang, Despina Louca, A Visinoiniu, S-H Lee, JD Thompson, T Proffen, A Llobet, Y Qiu, S Park, and Y Ueda. Local order and frustration in the geometrically frustrated spinels $\text{Cd}_{1-x}\text{Zn}_x\text{V}_2\text{O}_4$. *Physical Review B*, 74(1):014108, 2006.
- ¹⁶ Sian E Dutton, Qingzhen Huang, Oleg Tchernyshyov, CL Broholm, and RJ Cava. Sensitivity of the magnetic properties of the ZnCr_2O_4 and MgCr_2O_4 spinels to non-stoichiometry. *Physical Review B*, 83(6):064407, 2011.
- ¹⁷ SE Dutton, CL Broholm, and RJ Cava. Divergent effects of static disorder and hole doping in geometrically frustrated $\beta\text{-CaCr}_2\text{O}_4$. *Journal of Solid State Chemistry*, 183(8):1798–1804, 2010.
- ¹⁸ Masashige Onoda, Hiroyoshi Imai, Yasushi Amako, and Hiroshi Nagasawa. Spin fluctuation and the transport mechanism in vanadium oxide spinels with a metal-insulator transition. *Physical Review B*, 56(7):3760, 1997.
- ¹⁹ Keita Kobayashi, Masahiko Okumura, Susumu Yamada, Masahiko Machida, and Hideo Aoki. Superconductivity in repulsively interacting fermions on a diamond chain: Flat-band-induced pairing. *Physical Review B*, 94(21):214501, 2016.
- ²⁰ S Miyahara, S Kusuta, and N Furukawa. Bcs theory on a flat band lattice. *Physica C: Superconductivity*, 460:1145–1146, 2007.
- ²¹ A Mielke. Ferromagnetism in the hubbard model on line graphs and further considerations. *Journal of Physics A: Mathematical and General*, 24(14):3311, 1991.
- ²² A Mielke. Exact ground states for the hubbard model on the kagome lattice. *Journal of Physics A: Mathematical and General*, 25(16):4335, 1992.

- ²³ Shizhong Zhang, Hsiang-hsuan Hung, and Congjun Wu. Proposed realization of itinerant ferromagnetism in optical lattices. *Physical Review A*, 82(5):053618, 2010.
- ²⁴ I Hase, T Yanagisawa, Y Aiura, and K Kawashima. Possibility of flat-band ferromagnetism in hole-doped pyrochlore oxides $\text{Sn}_2\text{Nb}_2\text{O}_7$ and $\text{Sn}_2\text{Ta}_2\text{O}_7$. *Physical review letters*, 120(19):196401, 2018.
- ²⁵ Evelyn Tang, Jia-Wei Mei, and Xiao-Gang Wen. High-temperature fractional quantum hall states. *Physical review letters*, 106(23):236802, 2011.
- ²⁶ Zheng Liu, Zheng-Fei Wang, Jia-Wei Mei, Yong-Shi Wu, and Feng Liu. Flat chern band in a two-dimensional organometallic framework. *Phys. Rev. Lett.*, 110:106804, Mar 2013.
- ²⁷ Ninghai Su, Wei Jiang, Zhengfei Wang, and Feng Liu. Prediction of large gap flat chern band in a two-dimensional metal-organic framework. *Appl. Phys. Lett.*, 112(3):033301, January 2018.
- ²⁸ Wei Jiang, Meng Kang, Huaqing Huang, Hongxing Xu, Tony Low, and Feng Liu. Topological band evolution between lieb and kagome lattices. *Phys. Rev. B*, 99:125131, Mar 2019.
- ²⁹ Yinong Zhou, Kyung-Hwan Jin, Huaqing Huang, Zhengfei Wang, and Feng Liu. Weyl points created by a three-dimensional flat band. *Physical Review B*, 99(20):201105, 2019.
- ³⁰ See Supplemental Material at [URL will be inserted by publisher] for calculation methods, AFM band structure, band structure with different U, distorted octahedron field-splitting, double pyrochlore bands, energy difference between FM and AFM state under isotropic strain, bands after hole doping, and wannier90 fitted bands.
- ³¹ Anubhav Jain, Shyue Ping Ong, Geoffroy Hautier, Wei Chen, William Davidson Richards, Stephen Dacek, Shreyas Cholia, Dan Gunter, David Skinner, Gerbrand Ceder, et al. Commentary: The materials project: A materials genome approach to accelerating materials innovation. *Apl Materials*, 1(1):011002, 2013.
- ³² Sudhir K Pandey. Orbital ordering in the geometrically frustrated MgV_2O_4 : Ab initio electronic structure calculations. *Physical Review B*, 84(9):094407, 2011.
- ³³ Nicola Marzari and David Vanderbilt. Maximally localized generalized wannier functions for composite energy bands. *Physical review B*, 56(20):12847, 1997.
- ³⁴ Jiang et al. Giant anomalous hall effect due to double-degenerate quasi flat bands. *arXiv*, August 2020.
- ³⁵ Philip W Anderson. Ordering and antiferromagnetism in ferrites. *Physical Review*, 102(4):1008, 1956.
- ³⁶ H Mamiya, M Onoda, T Furubayashi, J Tang, and I Nakatani. Structural and magnetic studies on vanadium spinel MgV_2O_4 . *Journal of applied physics*, 81(8):5289–5291, 1997.
- ³⁷ J. Enkovaara, O. Heczko, A. Ayuela, and R. M. Nieminen. Coexistence of ferromagnetic and antiferromagnetic order in Mn-doped Ni_2MnGa . *Phys. Rev. B*, 67:212405, Jun 2003.
- ³⁸ J. S. White, M. Bator, Y. Hu, H. Luetkens, J. Stahn, S. Capelli, S. Das, M. Döbeli, Th. Lippert, V. K. Malik, J. Martynczuk, A. Wokaun, M. Kenzelmann, Ch. Niedermayer, and C. W. Schneider. Strain-induced ferromagnetism in antiferromagnetic LuMnO_3 thin films. *Phys. Rev. Lett.*, 111:037201, Jul 2013.
- ³⁹ Chan-Ho Yang, Daisuke Kan, Ichiro Takeuchi, Valanoor Nagarajan, and Jan Seidel. Doping BiFeO_3 : approaches and enhanced functionality. *Physical Chemistry Chemical Physics*, 14(46):15953–15962, 2012.
- ⁴⁰ Joonki Suh, Tae-Eon Park, Der-Yuh Lin, Deyi Fu, Joon-suk Park, Hee Joon Jung, Yabin Chen, Changhyun Ko, Chaun Jang, Yinghui Sun, et al. Doping against the native propensity of MoS_2 : degenerate hole doping by cation substitution. *Nano letters*, 14(12):6976–6982, 2014.